Golovanov, Dmitry and Galea, Michael and Gerada, C. (2017) High specific torque motor for propulsion system of aircraft. In: International Conference on Electrical Systems for Aircraft, Railway, Ship Propulsion and Road Vehicles & International Transportation Electrification Conference (ESARS-ITEC 2016), 2-4 November 2016, Toulouse, France.

High Specific Torque Motor for Propulsion System of Aircraft.

Dmitry Golovanov, Michael Galea, Chris Gerada
PEMC Research Group
The University of Nottingham
Nottingham, United Kingdom

***Abstract* – This paper proposes an analytical model that considers the torque characteristics for high specific torque synchronous machine with outer rotor and a Halbach permanent magnet array. The distribution of the magnetic field in the air gap is obtained with a linear assumption by solving Neumann's problem. The analytical model presented in the paper allows preliminary estimation and fast optimization of the machine's geometry and can be used to develop a first cut design of the machine.**

The application of the analytical model proposed is demonstrated via the adaptation and modification of a traction machine designed for electrical taxiing to a machine for propulsion of electric aircraft.

***Index Terms* – Analytical solution, Halbach array, permanent magnets.**

The concept of the more electric aircraft (MEA) pushes researchers to search for innovative topologies of electrical machines suitable for aircraft propulsion. At first glance, synchronous machines with permanent magnets (PMs) look the most attractive, in terms of meeting such demands of specific torque characteristics and efficiency [1, 2], in the short term future. One of the most promising topologies was presented in [3, 4, 5]. The so called green taxiing motor (GT) was developed for taxiing a medium range aircraft on the ground. The main advantage of this motor is an ability to reach highest specific torque in terms of torque-to-mass and torque-to-volume ratios. The studied GT motor concept involves application of outer rotor with Halbach PM array and using 3-phase double-star winding configuration [1]. The design of GT was optimized for low rotation speed – 120-180 rpm, high torque – 7 kNm, high specific torque – 64 Nm/kg and short-term operation in intermittent mode – 2000 s.

The main requirements for propulsion motors are high torque-density or power-density characteristics and high efficiency (>97%) at the speed of rotation, typically around 2500 rpm. The GT characteristics seem acceptable to satisfy the mentioned above requirements. Thereby, while the GT motor was originally designed for traction purposes, however the topology can be a good starting point for further investigation for optimal motor design of propulsion.

An analytical model can be a useful tool at the first stage of research. It allows doing a quick estimation of machines characteristics for a wide range of parameters: pole pairs, machine dimension, current load, size of PM, etc. At the same time the preliminary machine design optimization also can be performed by using the analytical model. This can result in a narrowed range for parameters for more accurate and time consuming optimization by applying finite element analysis (FEA).

This paper contains an analytical solution for the mentioned GT motor topology and shows results of the estimation of its specific power and specific torque characteristics as well as its efficiency. All this is shown, once the analytical model has been applied to 'convert' the optimal design for traction to a design more suitable for propulsion.

I. Solution of Magnetostatic Problem for Synchronous Motor with Halbach PM Array

The Halbach array is a well known structure of PMs which allows the increasing of flux density [4] of machines, mainly by improving the harmonic quality of the main air-gap flux. The Halbach magnetic cylinder gives the effect of concentration of magnetic flux for either outward or inward cylinder and can be used in synchronous machines with PM [7, 8]. The topology of this kind of synchronous machine with inner concentration of magnetic field is shown in Fig. 1. The Halbach cylinder is placed in between two ferromagnetic domains with infinite permeability. The inner ferromagnetic domain represents stator with winding described by discontinuous current sheet on the surface R_1.

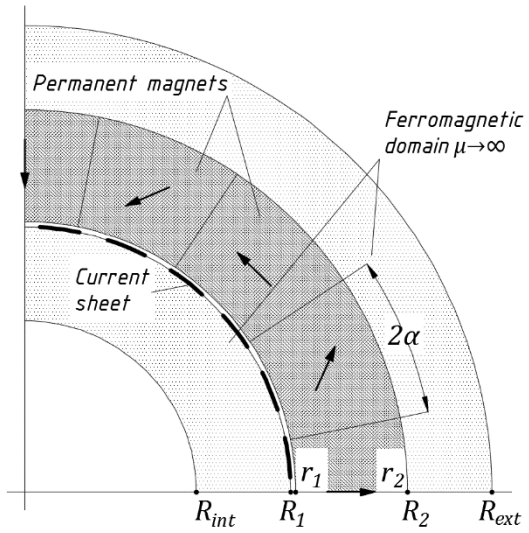

Fig. 1 – Outer rotor machine with Halbach PM array

In order to obtain an analytical solution of the magnetic field distribution for this kind of topology the following assumptions were taken:

- Stator domain and rotor yoke are described as ferromagnetic cylinders with infinite permeability $\mu \to \infty$ but without taking in account slotting effect - Fig. 1;
- The Halbach PM array consists of 4 magnets per pole pitch with 45° in between vectors of magnetization of neighboring magnets;
- The magnets have uniform magnetization $M = const$ with relative magnetic permeability $\mu_{mag} = 1$ - Fig. 1.
- The current in stator's winding is described as discontinuous current sheets on the surface of stator;
- Stator slots are not considered and replaced with smooth ferromagnetic surface
- The magnetic fields are plane-parallel and 3D effects are not considered;

The analytical solution of the magnetic field for this machine consists of sum of fields produced across the Halbach cylinder taking into account the influence of the ferromagnetic domains and field of the discontinuous current sheet.

A. The solution for isolated Halbach cylinder

Halbach cylinder consist of a sequence of PMs, magnetized in different directions – Fig. 2a. The considered cylinder has four periodically repeated PM elements (marked from 1 to 4 in Fig. 2a). The total field of cylinder was found as a sum of fields of these PM elements. Laplace and Poisson equations with appropriate boundary conditions showed in Fig. 2b were solved for each PM element in each domain (external domain: $r \geq r_2$, internal domain $0 \leq r \leq r_1$ and PM region $r_1 \leq r \leq r_2$) [9, 10].

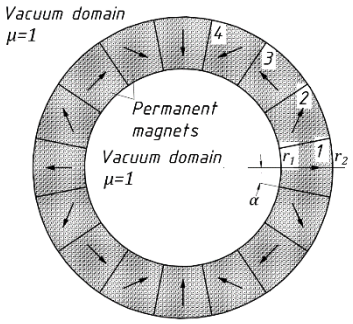

a) Halbach cylinder

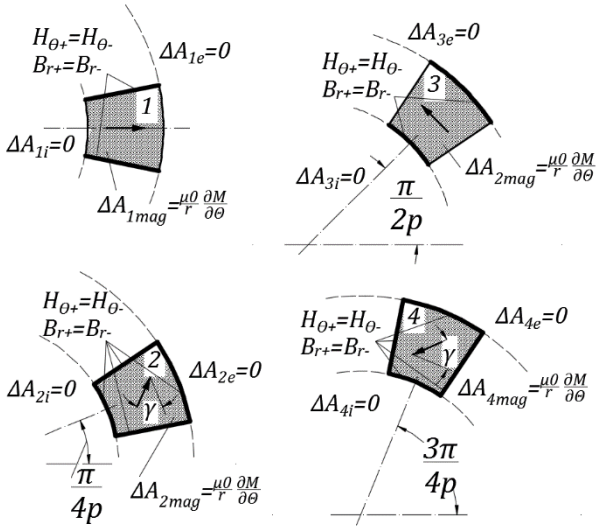

b) boundary conditions for isolated elements of Halbach cylinder

Fig. 2 – Schematic representation of magnetostatic problem for isolated Halbach cylinder

The result of the solution is presented for the internal region only. For the internal region $0 \leq r \leq r_1$ we have (1-4):

$$A_{1i} = \mu_0 \frac{2M}{\pi} \sum \frac{r^{pn}\left(r_2^{1-pn} - r_1^{1-pn}\right)}{n(1-pn)} sin(pn\theta)\, sin(pn\alpha) \quad (1)$$

$$A_{2i} = \mu_0 \frac{2M}{\pi} \sum \frac{r^{pn}\left(r_2^{1-pn} - r_1^{1-pn}\right)}{n(1-pn)} \left[cos\,\gamma\, sin\left(pn\left[\theta + \frac{\pi}{4p}\right]\right) cos\left(pn\left[\frac{\pi}{2p} - \alpha\right]\right) + sin\,\gamma\, sin\left(pn\left[\theta - \frac{\pi}{4p}\right]\right) sin(pn\alpha)\right] \quad (2)$$

$$A_{3i} = \mu_0 \frac{2M}{\pi} \sum \frac{r^{pn}\left(r_2^{1-pn} - r_1^{1-pn}\right)}{n(1-pn)} sin(pn\theta)\, cos\left(pn\left[\frac{\pi}{2p} - \alpha\right]\right) \quad (3)$$

$$A_{4i} = \mu_0 \frac{2M}{\pi} \sum \frac{r^{pn}\left(r_2^{1-pn} - r_1^{1-pn}\right)}{n(1-pn)} \left[cos\,\gamma\, sin\left(pn\left[\theta - \frac{\pi}{4p}\right]\right) cos\left(pn\left[\frac{\pi}{2p} - \alpha\right]\right) - sin\,\gamma\, sin\left(pn\left[\theta - \frac{3\pi}{4p}\right]\right) sin(pn\alpha)\right] \quad (4)$$

Here $0 \leq \alpha \leq \frac{\pi}{8p}$ – angle of PMs elements, $0 \leq \gamma \leq \frac{\pi}{2}$ – direction of magnetization of elements 2 and 4 – Fig. 2b.

B. The influence of the ferromagnetic region

The Fourier series (5) with coefficients C and B describes the influence of ferromagnetic domain.

$$A_{Fe3} = \sum \left(C r^{pn} + \frac{B}{r^{pn}}\right) \sin(pn\theta)\ \forall\ R_1 < r < R_2 \quad (5)$$

Coefficients C and B (8, 9) were received from the boundary conditions (6, 7).

$$\frac{\partial A_{\mathrm{Fe3}}}{\partial r} + \frac{\partial A_{1i}}{\partial r} + \frac{\partial A_{2i}}{\partial r} + \frac{\partial A_{3i}}{\partial r} + \frac{\partial A_{4i}}{\partial r}\Big|_{r=R_1,} = 0 \quad (6)$$

$$\frac{\partial A_{\mathrm{Fe3}}}{\partial r} + \frac{\partial A_{1e}}{\partial r} + \frac{\partial A_{2e}}{\partial r} + \frac{\partial A_{3e}}{\partial r} + \frac{\partial A_{4e}}{\partial r}\Big|_{r=R_2,} = 0 \quad (7)$$

$$C = \frac{\left(B\frac{1}{{R_1}^{pn+1}} - \mu_0 \frac{2M}{\pi} \frac{K_1(\theta)}{\sin(pn\theta)}\right)}{{R_1}^{pn-1}}, \quad (8)$$

$$B = \frac{\mu_0 \frac{2\mathrm{M}}{\pi}\left(K_2(\theta){R_1}^{pn-1} - K_1(\theta){R_2}^{pn-1}\right)}{\left[\frac{{R_1}^{pn-1}}{{R_2}^{pn+1}} - \frac{{R_2}^{pn-1}}{{R_1}^{pn+1}}\right]\sin(pn\theta)} \quad (9)$$

here $K_1(\theta)$ and $K_2(\theta)$ are defined as (10, 11).

$$K_1(\theta) = \frac{{R_1}^{pn-1}\left(r_2^{1-pn} - r_1^{1-pn}\right)}{n(1-pn)}\left\{cos\,\gamma\, cos\left(pn\left[\frac{\pi}{2p} - \alpha\right]\right)\cdot\left[sin\left(pn\left[\theta + \frac{\pi}{4p}\right]\right) + sin\left(pn\left[\theta - \frac{\pi}{4p}\right]\right)\right] + sin\,\gamma\, sin(pn\alpha)\cdot \left[sin\left(pn\left[\theta - \frac{\pi}{4p}\right]\right) - sin\left(pn\left[\theta - \frac{3\pi}{4p}\right]\right)\right] + sin(pn\theta)\cdot\left[sin(pn\alpha) + cos\left(pn\left[\frac{\pi}{2p} - \alpha\right]\right)\right]\right\} \quad (10)$$

$$K_2(\theta) = \frac{{R_2}^{-pn-1}\left(r_2^{1+pn} - r_1^{1+pn}\right)}{n(1+pn)}\left\{cos\,\gamma\, cos\left(pn\left[\frac{\pi}{2p} - \alpha\right]\right)\cdot\left[sin\left(pn\left[\theta + \frac{\pi}{4p}\right]\right) + sin\left(pn\left[\theta - \frac{\pi}{4p}\right]\right)\right] - sin\,\gamma\, sin(pn\alpha)\cdot \left[sin\left(pn\left[\theta - \frac{3\pi}{4p}\right]\right) - sin\left(pn\left[\theta - \frac{\pi}{4p}\right]\right)\right] + sin(pn\theta)\cdot\left[cos\left(pn\left[\frac{\pi}{2p} - \alpha\right]\right) - sin(pn\alpha)\right]\right\} \quad (11)$$

C. *Solution for ferromagnetic yoke*

The expressions (12, 13) give the description of distribution of magnetic field within external ($R_2 < r < R_{ext}$) and internal ($R_{int} < r < R_1$) ferromagnetic yokes.

$$A_{yoke\_ext} = \sum\left(U_1 r^{pn} + \frac{U_2}{r^{pn}}\right) sin(pn\theta)\ \ R_2 < r < R_{ext} \quad (12)$$

$$A_{yoke\_int} = \sum\left(U_3 r^{pn} + \frac{U_4}{r^{pn}}\right) sin(pn\theta)\ \ R_{int} < r < R_1 \quad (13)$$

Taking into account boundary conditions (14 - 17) coefficients U_1, U_1, U_4, U_3 can be defined as (18 - 21) respectively.

$$\text{at } r = R_{int}\text{: } A_{yoke\_int} = 0 \quad (14)$$

$$\text{at } r = R_1\text{: } A_{yoke\_int} = A_{1i} + A_{2i} + A_{3i} + A_{4i} + A_{Fe3} \quad (15)$$

$$\text{at } r = R_2\text{: } A_{yoke\_ext} = A_{1e} + A_{2e} + A_{3e} + A_{4e} + A_{Fe3} \quad (16)$$

$$\text{at } r = R_{ext}\text{: } A_{yoke\_ext} = 0 \quad (17)$$

$$U_2 = -\frac{\left(A_{Fe3}(R_2,\theta) + A_{1e}(R_2,\theta) + A_{2e}(R_2,\theta) + A_{3e}(R_2,\theta) + A_{4e}(R_2,\theta)\right)R_{ext}^{pn}}{sin(pn\theta)\left[\left(\frac{R_2}{R_{ext}}\right)^{pn} - \left(\frac{R_{ext}}{R_2}\right)^{pn}\right]} \quad (18)$$

$$U_1 = -\frac{U_{12}}{R_{ext}^{2pn}} \quad (19)$$

$$U_4 = -\frac{\left(A_{\mathrm{Fe}3}(R_1,\theta) + A_{1i}(R_1,\theta) + A_{2i}(R_1,\theta) + A_{3i}(R_1,\theta) + A_{4i}(R_1,\theta)\right)R_{int}^{pn}}{sin(pn\theta)\left[\left(\frac{R_1}{R_{int}}\right)^{pn} - \left(\frac{R_{int}}{R_1}\right)^{pn}\right]} \quad (20)$$

$$U_3 = -\frac{U_{14}}{R_{int}^{2pn}} \quad (21)$$

II. SOLUTION OF MAGNETOSTATIC PROBLEM FOR DOUBLE STAR DISCONTINUOUS CURRENT SHEET

A double-star 3-phase winding was implemented in the GT motor to reduce the torque pulsations and simplify the coils design. The double star concept involves the use of two sets of 3-phase windings with 30° shift in between of sets, powered by two separate converters and with a common star-point [5]. With the implementation of such a 'double star' system, improvements in the torque ripple can be achieved. Due to the suystem having a common star point (for both 3-phase systems) no extra losses are incurred.

For the analytical model, the three phase stator windings can be described as discontinuous current sheets on the surfaces of ferromagnetic region R_2 – Fig. 3. The field of the current sheet is described as a superposition of the fields of currents - J_{S1_A}, J_{S1_B}, J_{S1_C}, and - J_{S2_A}, J_{S2_B}, J_{S2_C}, respectively, which represents the double star winding - Fig. 3.

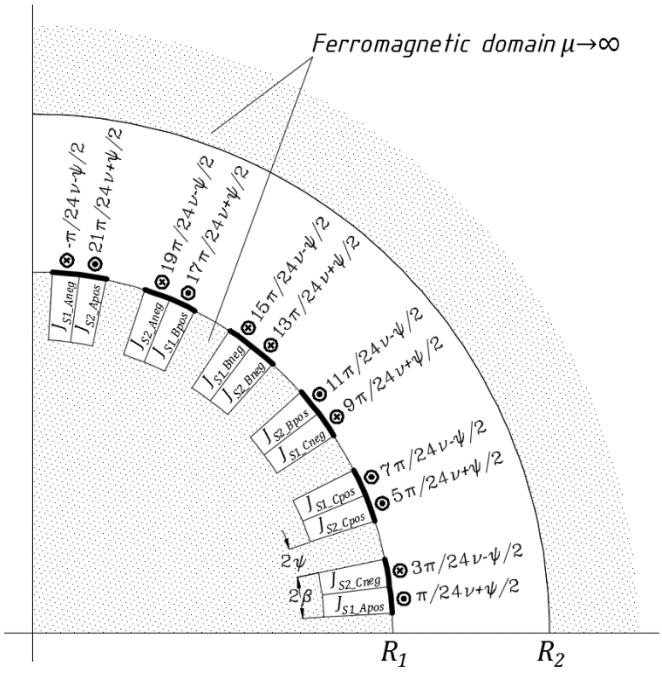

Fig. 3 – Schematic representation of magnetostatic problem for discontinuous current sheet

The current J_{S1_A} can be represented as a Fourier series (22), (23) for a positive and negative current direction in the coil. The angular position of current sheet elements can be found in Fig. 3.

$$J_{S1\_Apos} = \frac{4J_0}{\pi}\sum\frac{1}{n}cos\left(\nu n\left[\theta - \frac{\pi}{24\nu} - \frac{\psi}{2} + \theta_0\right]\right) sin(\nu n\beta) \quad (22)$$

$$J_{S1\_Aneg} = -\frac{4J_0}{\pi}\sum\frac{1}{n}cos\left(\nu n\left[\theta + \frac{\pi}{24\nu} + \frac{\psi}{2} + \theta_0\right]\right) sin(\nu n\beta) \quad (23)$$

here J_0 – peak value of current load, θ_0 – power angle, β – coil angle, ψ – tooth angle, ν – number of coils per phase, – Fig. 3.

The magnetic field in between R_1 and R_2 is described by Laplace equation (24) with boundary conditions (25, 26).

$$\Delta A_{S1\_Apos} = 0 \quad (24)$$

$$\text{at } r = R_1\text{: } \frac{\partial \Delta A_{S1\_Apos}}{\partial r} = \mu_0 J_{S1\_Apos} \quad (25)$$

$$\text{at } r = R_2\text{: } \frac{\partial \Delta A_{S1\_Apos}}{\partial r} = 0 \quad (26)$$

The expression (27) can be obtained after solving (24 - 26). The same analytical approach as for current J_{S1_Apos} had been applied for other current and results are shown below – (28 – 38). The total field produced by current sheet Fig. 3 is a sum of separately solutions (27 – 38).

$$A_{S1\_Apos} = -K_{S1A}\sum\frac{1}{n^2}\left[(a_n + 1)\left(\frac{r}{R_1}\right)^{-pn} + (a_n - 1)\left(\frac{R_1}{r}\right)^{-pn}\right] cos\left(pn\left[\theta - \frac{\pi}{24\nu} - \frac{\psi}{2} + \theta_0\right]\right) sin(pn\beta) \quad (27)$$

$$A_{S1\_Aneg} = K_{S1A}\sum\frac{1}{n^2}\left[(a_n+1)\left(\frac{r}{R_1}\right)^{-pn}+(a_n-1)\left(\frac{R_1}{r}\right)^{-pn}\right]cos\left(pn\left[\theta+\frac{\pi}{24\nu}+\frac{\psi}{2}+\theta_0\right]\right)sin(pn\beta) \quad (28)$$

$$A_{S2\_Apos} = -K_{S2A}\sum\frac{1}{n^2}\left[(a_n+1)\left(\frac{r}{R_1}\right)^{-pn}+(a_n-1)\left(\frac{R_1}{r}\right)^{-pn}\right]cos\left(pn\left[\theta-\frac{21\pi}{24\nu}-\frac{\psi}{2}+\theta_0\right]\right)sin(pn\beta) \quad (29)$$

$$A_{S2\_Aneg} = K_{S2A}\sum\frac{1}{n^2}\left[(a_n+1)\left(\frac{r}{R_1}\right)^{-pn}+(a_n-1)\left(\frac{R_1}{r}\right)^{-pn}\right]cos\left(pn\left[\theta-\frac{19\pi}{24\nu}+\frac{\psi}{2}+\theta_0\right]\right)sin(pn\beta) \quad (30)$$

$$A_{S1\_Bpos} = K_{S1B}\sum\frac{1}{n^2}\left[(a_n+1)\left(\frac{r}{R_1}\right)^{-pn}+(a_n-1)\left(\frac{R_1}{r}\right)^{-pn}\right]cos\left(pn\left[\theta-\frac{17\pi}{24\nu}-\frac{\psi}{2}+\theta_0\right]\right)sin(pn\beta) \quad (31)$$

$$A_{S1\_Bneg} = -K_{S1B}\sum\frac{1}{n^2}\left[(a_n+1)\left(\frac{r}{R_1}\right)^{-pn}+(a_n-1)\left(\frac{R_1}{r}\right)^{-pn}\right]cos\left(pn\left[\theta-\frac{15\pi}{24\nu}+\frac{\psi}{2}+\theta_0\right]\right)sin(pn\beta) \quad (32)$$

$$A_{S2\_Bpos} = K_{S2B}\sum\frac{1}{n^2}\left[(a_n+1)\left(\frac{r}{R_1}\right)^{-pn}+(a_n-1)\left(\frac{R_1}{r}\right)^{-pn}\right]cos\left(pn\left[\theta-\frac{13\pi}{24\nu}+\frac{\psi}{2}+\theta_0\right]\right)sin(pn\beta) \quad (33)$$

$$A_{S2\_Bneg} = -K_{S2B}\sum\frac{1}{n^2}\left[(a_n+1)\left(\frac{r}{R_1}\right)^{-pn}+(a_n-1)\left(\frac{R_1}{r}\right)^{-pn}\right]cos\left(pn\left[\theta-\frac{11\pi}{24\nu}-\frac{\psi}{2}+\theta_0\right]\right)sin(pn\beta) \quad (34)$$

$$A_{S1\_Cpos} = K_{S1C}\sum\frac{1}{n^2}\left[(a_n+1)\left(\frac{r}{R_1}\right)^{-pn}+(a_n-1)\left(\frac{R_1}{r}\right)^{-pn}\right]cos\left(pn\left[\theta-\frac{9\pi}{24\nu}+\frac{\psi}{2}+\theta_0\right]\right)sin(pn\beta) \quad (35)$$

$$A_{S1\_Cneg} = -K_{S1C}\sum\frac{1}{n^2}\left[(a_n+1)\left(\frac{r}{R_1}\right)^{-pn}+(a_n-1)\left(\frac{R_1}{r}\right)^{-pn}\right]cos\left(pn\left[\theta-\frac{7\pi}{24\nu}-\frac{\psi}{2}+\theta_0\right]\right)sin(pn\beta) \quad (36)$$

$$A_{S2\_Cpos} = K_{S2C}\sum\frac{1}{n^2}\left[(a_n+1)\left(\frac{r}{R_1}\right)^{-pn}+(a_n-1)\left(\frac{R_1}{r}\right)^{-pn}\right]cos\left(pn\left[\theta-\frac{5\pi}{24\nu}-\frac{\psi}{2}+\theta_0\right]\right)sin(pn\beta) \quad (37)$$

$$A_{S2\_Cneg} = -K_{S2C}\sum\frac{1}{n^2}\left[(a_n+1)\left(\frac{r}{R_1}\right)^{-pn}+(a_n-1)\left(\frac{R_1}{r}\right)^{-pn}\right]cos\left(pn\left[\theta-\frac{3\pi}{24\nu}+\frac{\psi}{2}+\theta_0\right]\right)sin(pn\beta) \quad (38)$$

Where:

$K_{S1A} = 2\mu_0 i_0 w_a$, $K_{S2A} = \frac{\sqrt{3}}{2}\mu_0 i_0 w_a$, $K_{S1B} = \frac{1}{2}\mu_0 i_0 w_a$, $K_{S2B} = 0$, $K_{S1C} = \frac{1}{2}\mu_0 i_0 w_a$, $K_{S2C} = \frac{\sqrt{3}}{2}\mu_0 i_0 w_a$. These coefficients are given for the starting time $t = 0$, where we have $J_{S1A} = J_0$, $J_{S1B} = J_{S1C} = -\frac{1}{2}J_0$ and $J_{S2A} = J_{S2C} = \frac{\sqrt{3}}{2}J_0$, $J_{S2B} = 0$.

$n = 1,3..$ – odd harmonics, $0 \le \beta \le \frac{\pi}{6\nu}$, θ_0– power angle, ν – pole-pairs from current sheet, i_0 – peak phase current, w_a – number of turns per one coil of phase, coefficient a_n was defined from boundary conditions (25 – 26) and expressed as (39)

$$a_n = -\frac{R_1^{2\nu n}+R_2^{2\nu n}}{R_1^{2\nu n}-R_2^{2\nu n}} \quad (39)$$

III. Comparison Analytical and FEA Results and Torque Characteristics

The analytical and FEA computations had been performed with GT motor parameters listed in Table 1. The analytical model was compared with FEA solution at different conditions:

- linear assumption of steel permeability and without taking into account slotting effect;
- linear assumption with slotting effect;
- nonlinear assumption with slotting effect.

TABLE I Parameters of the outer rotor machine with Halbach array

Parameter	Symbol	Value	Unit
Magnetization of PMs	M	*775*	kA/m
Relative permeability of PMs	μ_{mag}	*1*	-
Number of pole pairs	p	*21*	-
Internal radius of stator	R_{int}	*142*	*mm*
External radius of stator	R_1	*203.5*	*mm*
Internal radius of outer ring	R_2	*225*	*mm*
External radius of outer ring	R_{ext}	*235*	*mm*
Internal radius of PMs cylinder	r_1	*205*	*mm*
External radius of PMs cylinder	r_2	*225*	*mm*
Angle of PMs element	α	$\frac{\pi}{8p}$ *(3.75°)*	*degrees*
Phase peak current	i_0	225	*A*
Coil turns	w_a	33	-

The common distribution of the magnetic flux lines within active part of GT motor at no-load conditions for analytical computation; for FEA without slots; and– for FEA with slots, is shown in Fig. 4a; Fig. 4b; Fig. 4c, respectively. As can be seen from the Fig 4 the slots cause significant redistribution of magnetic field in active part of machine in comparison with nonslots case.

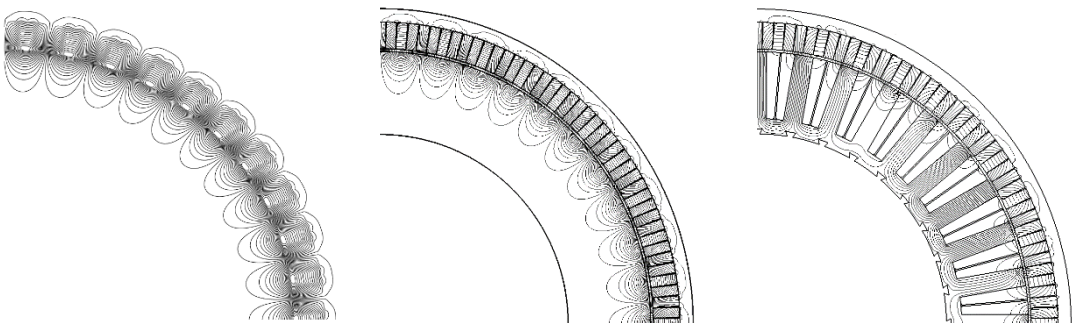

a) Analytical b) FEA without slots c) FEA with slots

Fig. 4 – The distribution of magnetic flux lines within active part of GT motor for nonload condition

The comparison of magnetic flux density distribution in the air gap of machine obtained from analytical and FEA solutions are given in Fig. 5a, b. The results are shown for radial component of flux density at lineal assumption of stator material permeability without considering slots – Fig. 5a and with slotting effect – Fig. 5b. Very good agreement can be observed in case of slots absence– Fig. 5a. When taking into account the stator's open slots, a significant difference between analytical and FEA results occur. This is shown in Fig 5b.

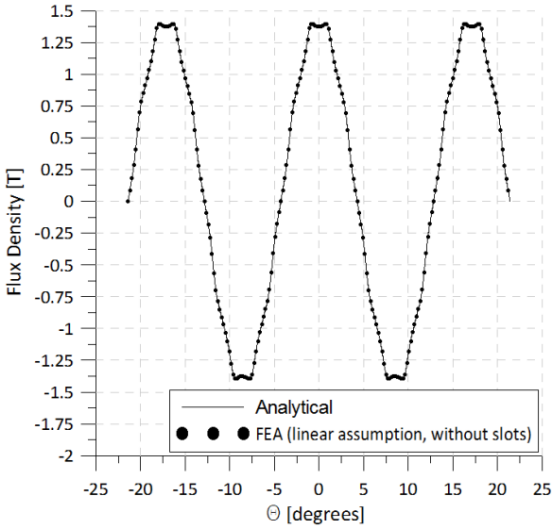

a) linear assumption, without slotting effect

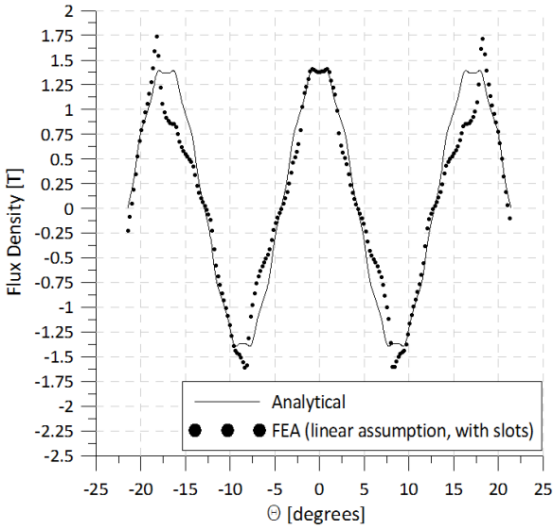

b) linear assumption, FEA solution with slotting effect

Fig. 5 – Radial component of flux density in the air gap for nonload condition

The torque performance of the GT motor was estimated analytically by using Maxwell stress tensor (40) and compared with FEA results at different conditions – Fig. 6.

$$T_i = \frac{L_a R_{i\_m}^2}{\mu_0} \int_0^{2\pi} B_{r\_i}\left(R_{i\_m}, \theta\right) B_{\theta\_i}\left(R_{i\_m}, \theta\right) d\theta \qquad (40)$$

The analytical solution gives good agreement with FEA in case of considering smooth stator surface (no slots) at linear assumption. The difference can be seen in case of considering open slots in FEA model. At peak phase current 225 A the difference in torque caused by opened slots is 13.5%. So, the open slots have significant influence on field distribution and thus on torque.

It should be also mentioned that GT motor is a highly saturated machine due to the high current load. Taking into account the nonlinear properties of stator material (Vacoflux 50, 0.35 mm laminations) the difference between analytical result and FEA reaches 33% - Fig. 6.

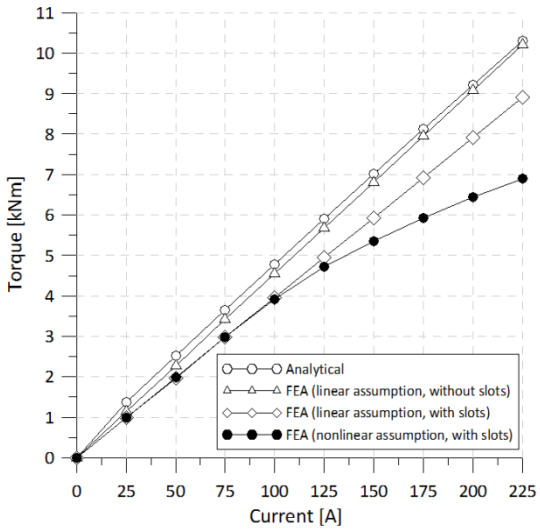

Fig. 6 – Torque characteristic ($M = 775\frac{kA}{m}$, $p = 21, \alpha = \frac{\pi}{8p}, \theta_0 = \pi/2p, n = 21$)

The nominal RMS current density of GT motor at reference speed 120 – 180 rpm is 26 A/mm^2 that allows reaching 64 Nm/kg (for the inactive materials only) of specific torque at short term operation. While such a current density, might seem quite high at first glance, however in the real application, this is mitigated by implementing a highly efficient, thermal management technique [6].

The specific torque and specific power as well as the total losses and efficiency of the original GT motor were estimated at 2500 rpm, in order to verify its potential in terms of a conversion for propulsion activities. The results were obtained from FEA and are given in Fig 7, 8. The total losses nonlinearly rise mainly due to Ohmic and eddy current losses and reach 55 kW at 26 A/mm^2 - Fig 7. Eddy current losses can be reduced by applying less thickness stator laminations which originally were 0.35 mm. The specific torque which has nonlinear correlation with current density rises from 9 Nm/kg at 3 A/mm^2 to 64 Nm/kg at 26 A/mm^2 of current density.

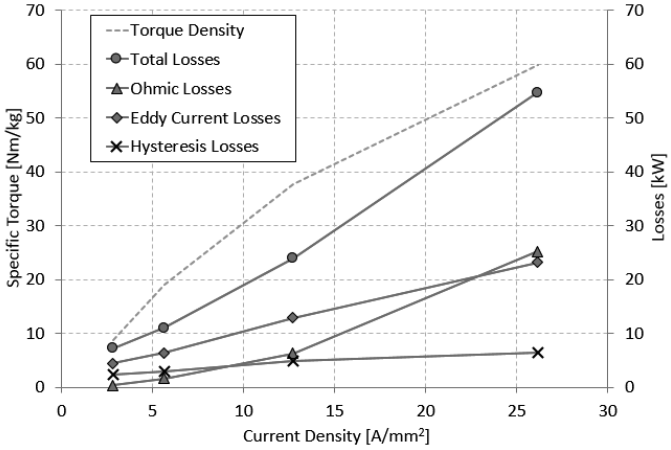

Fig. 7 – Specific torque and Losses characteristics (at 2500 rpm)

The specific power and efficiency characteristics of the GT motor at 2500 rpm are shown in Fig. 8. The efficiency of the motor is higher than 97% in the wide range of current load. For the nominal value of motor current density 26 A/mm^2 it is ~96.8% wherein specific power riches ~15.8 kW/kg. It also should be mentioned that the power of the GT machine at 2500 rpm and nominal current density 26 A/mm^2 is 1.7 MW. As it was mentioned above, the efficiency of GT still can be increased by redisign and optimization of its topology for high frequency and high rotation speed.

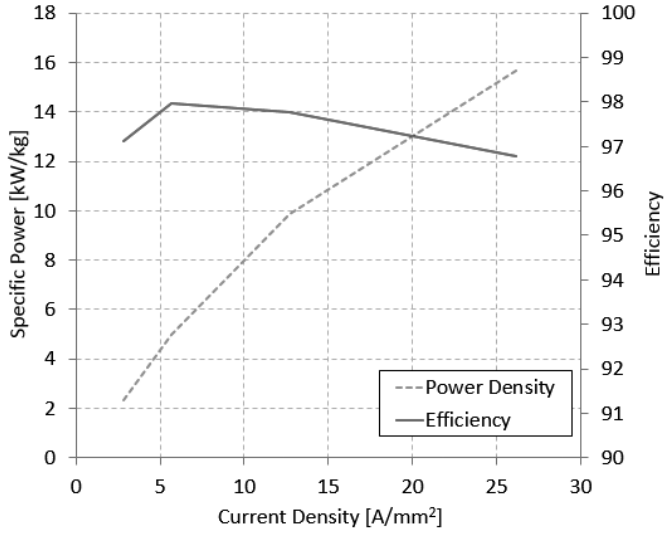

Fig. 8 – Specific power and efficiency characteristics (at 2500 rpm)

It should be mentioned that the GT works in intermittent mode with a maximum duration of 2500 seconds, which leads to periodic thermal heating. The original design of the GT included the use of forced air cooling, aided by other thermal management techniques as illustrated in [6]. The air flow passes through cooling radiator that is placed on the inner stator surface R_{int} above in Fig. 1. The estimation of thermal state of GT was presented in [3-5]. When upgrading the original technology to propulsion, then the 'normal' steady state operation, indicates that a liquid cooling system would be more promising and feasible.

IV. CONCLUSION

The description of the analytical model based on a solution of Laplace and Poisson equations for synchronous machine with a Halbach array are given in this paper. The models allow performing the calculation of magnetic field distribution within active parts of machine as well as estimation of torque characteristic. They give good agreement in case of non-slotting geometry of the stator. The models can be extremely useful at the first stage of research for the described topology as well as for the design and optimization of the machines' magnetic circuit when a linear assumption for different number of pole pairs, PM dimension, stator dimension, direction and amplitude of PM magnetization and current load is taken.

The simulation of the GT traction motor topology for the purpose of electric aircraft propulsion was also demonstrated. The simulated GT motor (applied with propulsion operation characteristics) can provide a high specific power (up to 15.8 kW/kg) and specific torque (up to 64 Nm/kg) characteristics at keeping efficiency higher than 97%. Thereby, all this confirms that the GT topology can be considered for further investigation from the standpoint of applying it as a motor for propulsion of electric aircraft.

V. REFERENCES

[1] M. Galea, L. Papini, H. Zhang, C. Gerada, and T. Hamiti, "Demagnetization Analysis for Halbach Array Configurations in Electrical Machines," *Magnetics, IEEE Transactions on,* vol. 51, pp. 1-9, 2015.

[2] Bulent Sarlioglu, Casey T. Morris "More Electric Aircraft: Review, Challenges, and Opportunities for Commercial Transport Aircraft" IEEE TRANSACTIONS ON TRANSPORTATION ELECTRIFICATION, VOL. 1, NO. 1, JUNE 2015

[3] M. Galea, Z. Xu, C. Tighe, T. Hamiti, C. Gerada, and S. Pickering, "Development of an aircraft wheel actuator for green taxiing," in Electrical Machines (ICEM), 2014 International Conference on, 2014, pp. 2492-2498.

[4] T. Raminosoa, T. Hamiti, M. Galea, and C. Gerada, "Feasibility and electromagnetic design of direct drive wheel actuator for green taxiing," in *Energy Conversion Congress and Exposition (ECCE), 2011 IEEE*, 2011, pp. 2798-2804.

[5] M. Galea, "High Performance, Direct Drive Machines for Aerospace Applications," PhD, Faculty of Engineering, University of Nottingham, UK, 2013.

[6] M. Galea, C. Gerada, T. Raminosoa, and P. Wheeler, "A Thermal Improvement Technique for the Phase Windings of Electrical Machines," *Industry Applications, IEEE Transactions on,* vol. 48, pp. 79-87, 2012.

[7] Z. Q. Zhu and D. Howe, "Halbach permanent magnet machines and applications: a review," Electric Power Applications, IEE Proceedings - , vol. 148, pp. 299-308, 2001.

[8] Yang Shen, Zi-Qiang Zhu, "General analytical model for calculating electromagnetic performance of permanent magnet brushless machines having segmented Halbach array"

[9] D. Golovanov, "Synchronous high temperature superconductor motors with permanent magnets", PhD. Thesis, Moscow aviation institute, 2010.

[10] L. Kovalev, Y. Kavun, D. Golovanov. "The limiting characteristics of synchronous machines with permanent magnets and high-temperature superconductors" // Electricity – 2008. – №12